

Recurrent ZNF83-E293V Mutation Promotes Bladder Cancer Progression through the NF- κ B Pathway via Transcriptional Dysregulation of S100A8

Zhao J. Lyu,^{1,2,15} Ying Wang,^{1,2,3,4,15} Jin L. Huang,^{2,5} Miao Chen,² Sha Y. Wu,² Qian Yan,² Yu Zhang,² Ying Tang,² Chen Jiang,^{4,5} Lei Li,^{2,4} Yi Z. Jia,⁶ Yu C. Liu,⁷ Hong B. Mei,⁸ Feng Wang,⁸ Ren H. Li,⁹ Ya C. Chen,¹⁰ Xiang Lin,¹¹ Zhi M. Cai,^{7,12,13,14} and Xin Y. Guan^{1,2,4}

¹Department of Clinical Oncology, The University of Hong Kong-Shenzhen Hospital, Shenzhen 518029, China; ²Department of Clinical Oncology, Li Ka Shing Faculty of Medicine, The University of Hong Kong, Hong Kong 999077, China; ³Department of Radiation Oncology, Sun Yat-Sen University Cancer Center, Guangzhou 510030, China; ⁴State Key Laboratory of Oncology in South China, Sun Yat-Sen University Cancer Center, Guangzhou 510030, China; ⁵Department of Pathology, Sun Yat-Sen University Cancer Center, Guangzhou 510030, China; ⁶Core Laboratory, The University of Hong Kong-Shenzhen Hospital, Shenzhen 518029, China; ⁷Guangdong Key Laboratory of Systems Biology and Synthetic Biology for Urogenital Tumors, Shenzhen Second People's Hospital, The First Affiliated Hospital of Shenzhen University, Shenzhen 518029, China; ⁸Department of Urology, Shenzhen Second People's Hospital, The First Affiliated Hospital of Shenzhen University, Shenzhen 518029, China; ⁹Shenzhen Institutes of Advanced Technology, Chinese Academy of Sciences, Shenzhen 518055, China; ¹⁰Department of Pathology, Shenzhen University General Hospital, Shenzhen 518055, China; ¹¹School of Chinese Medicine, The University of Hong Kong, Hong Kong 999077, China; ¹²Department of Urology, The First Affiliated Hospital of Shantou University Medical College, Shantou 515041, China; ¹³Carson International Cancer Center, School of Medicine, Shenzhen University, Shenzhen 518061, China; ¹⁴BGI-Medicine, BGI, Shenzhen 518083, China

Urothelial carcinoma (UC) is the predominant form of bladder cancer. Significant molecular heterogeneity caused by diverse molecular alterations brings about large variations in the response to treatment in UC. An improved understanding of the genetic mechanisms underlying the development and progression of UC is essential. Through deep analysis of next-generation sequencing data of 99 UC patients, we found that 18% of cases had recurrent somatic mutations in zinc finger protein gene zinc finger protein 83 (ZNF83). ZNF83 mutations were correlated with poor prognosis of UC. We also found a hotspot mutation, p.E293V, in the evolutionarily well-conserved region of ZNF83. ZNF83-E293V increased tumor growth and reduced the apoptosis of UC cells compared to wild-type ZNF83 both *in vitro* and in mice xenografted tumors. ZNF83-E293V activated nuclear factor κ B (NF- κ B) more potently than did the wild-type protein owing to its decreased transcriptional repression for S100A8. The NF- κ B inhibitors could pharmacologically block the tumor growth in mice engrafted with ZNF83-E293V-transfected UC cells. These findings provide a mechanistic insight and a potential therapeutic strategy for UC, which established a foundation for using the ZNF83-E293V mutation as a predictive biomarker of therapeutic response from NF- κ B inhibitors.

INTRODUCTION

Genomic mutation is a major hallmark of cancer.¹ The numbers of somatic DNA alterations displayed in bladder cancer were more than any adult genitourinary malignancies.² As the predominant form of bladder cancer, nearly 75% of urothelial carcinoma (UC)

were non-muscle-invasive bladder cancer (NMIBC), and 25% of UC patients present with muscle-invasive bladder cancer (MIBC) in the first diagnosis. The high frequency of recurrence in NMIBC and poor survival rate in MIBC emphasize the need for novel therapeutic approaches.^{3–5} Meanwhile, the significant molecular heterogeneity caused by diverse molecular alterations bring about large variation in the response to treatment in UC.⁶ An improved understanding of the genetic mechanisms underlying the development and progression of UC is essential.

With an increasing number of high-throughput sequencing studies, an accumulation of recurrent mutations has been identified in UC. For instance, fibroblast growth factor receptor 3 (FGFR3) and tumor protein p53 (TP53) were found to be the most frequently mutated genes in low-grade and high-grade UC, respectively.⁷ Previously, we identified genetic alterations of the chromatin remodeling genes in 59% of 97 subjects with UC.⁸ In a more recent sequencing study of 99 subjects with UC, we found that 32% of cases had genetic mutations in the process of sister chromatid cohesion and segregation.⁹ Recently, the advent of new therapies such as the first personalized

Received 6 February 2020; accepted 1 September 2020;
<https://doi.org/10.1016/j.ymthe.2020.09.004>.

¹⁵These authors contributed equally to this work.

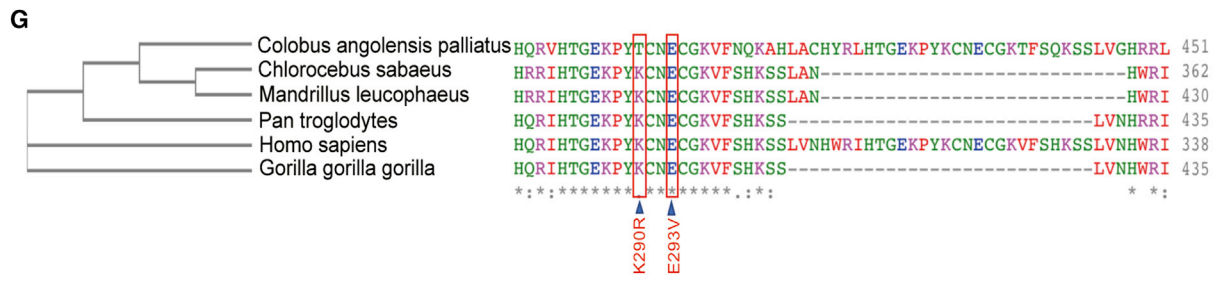
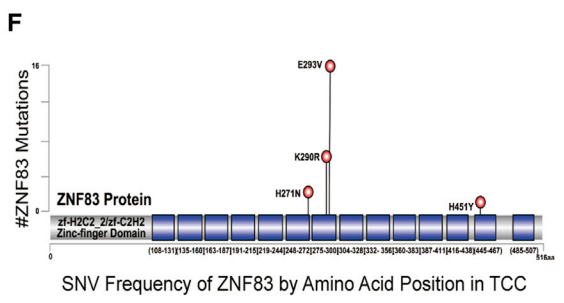
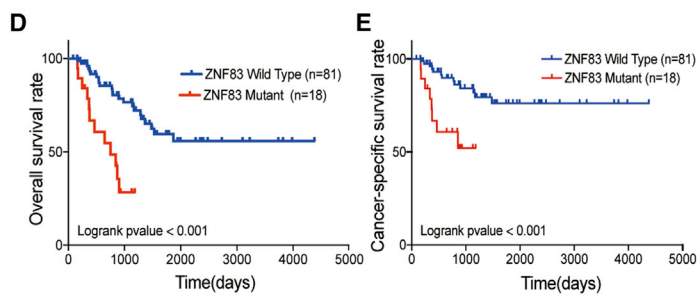
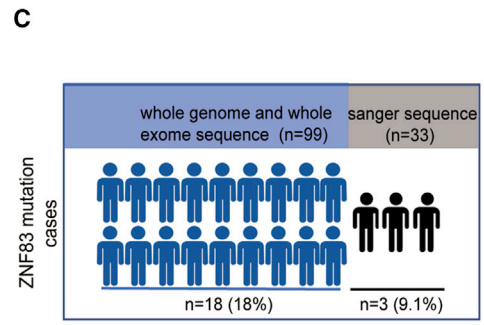
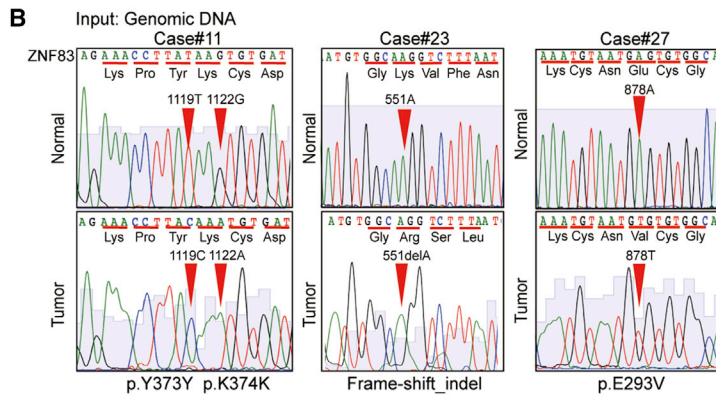
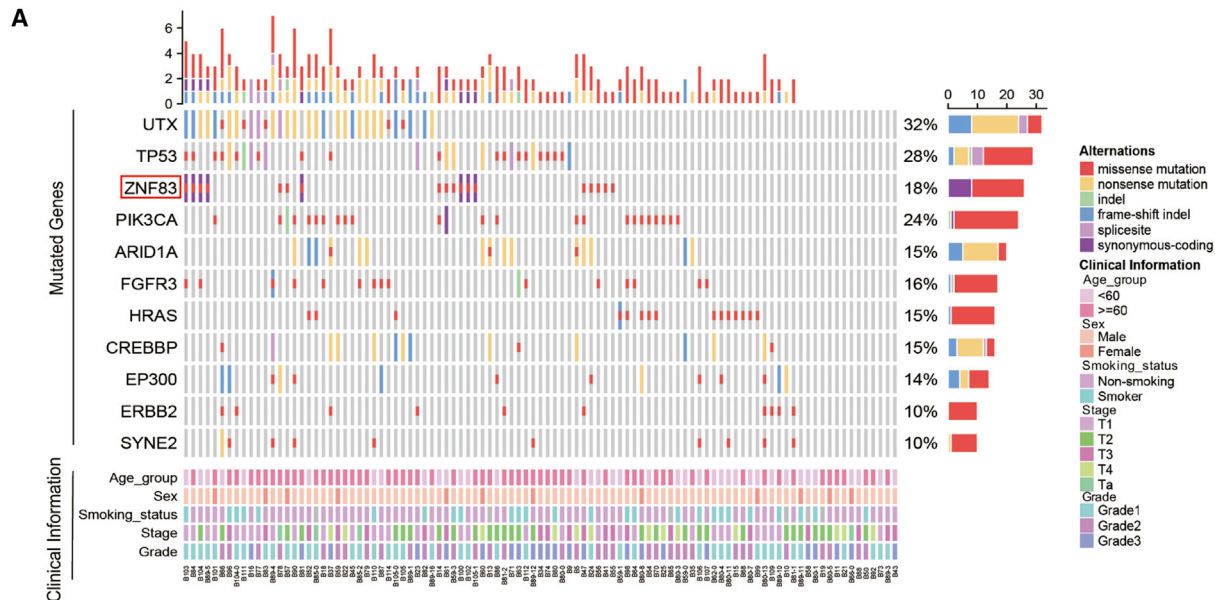
Correspondence: Xin Y. Guan, Department of Clinical Oncology, Li Ka Shing Faculty of Medicine, The University of Hong Kong, Hong Kong 999077, China.

E-mail: xyguan@hku.hk

Correspondence: Zhi M. Cai, Guangdong Key Laboratory of Systems Biology and Synthetic Biology for Urogenital Tumors, Shenzhen Second People's Hospital, The First Affiliated Hospital of Shenzhen University, Shenzhen 518029, China.

E-mail: caizhiming2000@163.com





(legend on next page)

drug targeting the key driver genetic alterations in FGFRs and the antibody-drug conjugate targeting Nectin-4 have shown promising clinical benefits in the treatment of patients with progressive bladder cancer.¹⁰ These breakthroughs further highlighted the importance of a deep understanding of the substantial mutated genes of UC.

In this study, with an in-depth analysis of our sequencing data, we identified a mutated gene, zinc finger protein 83 (ZNF83), which harbored somatic mutations in 18 of 99 of all samples. Overrepresentation of the genetic variants in tumor is a strong indicator of functional importance in cancer progression.¹¹ Nevertheless, little research has been done on the role of ZNF83 in UC or other diseases so far. The present study set out to investigate the biological function and molecular mechanism of ZNF83 mutation in UC development, which might provide a biomarker with therapeutic potential or prognostic value in UC.

RESULTS

Somatic Mutations of ZNF83 Were Frequently Detected in UC and Correlated with Poor Prognosis

To identify potential driver genetic alterations in UC, we re-analyzed the sequencing data of 99 UC samples. In total, we identified 11 genes with mutation rates above 10% in 99 cases, all of which have already been reported in previous studies, except for ZNF83. The missense mutation rate of ZNF83 reached 18% (Figure 1A), and the recurrent genetic alterations of ZNF83 were subsequently confirmed by Sanger sequencing, in which three somatic mutations of an additional 33 formalin-fixed, paraffin-embedded (FFPE) and the paired normal specimens were identified (Figure 1B). The frequent mutation of ZNF83 was also validated in other studies with big data analysis by cBioPortal (<http://www.cbioportal.org>) (Figures S1A and S1C).¹² Apart from bladder cancer, small-cell lung cancer (SCLC) and UC also harbored relatively higher mutation rates of ZNF83 compared to other cancer types. The big data analysis from high-performance integrated virtual environment (HIVE) biochemistry also validated that bladder cancer harbored high mutation rates of ZNF83 (Figure S1B).¹³ In total, ZNF83 mutations were detected in 18 of 99 cases by whole-genome and whole-exome sequencing and validated in 3 of 33 cases by Sanger sequencing (Figure 1C; Table S1 and S2).

ZNF83 is located in 19q13.41.¹⁴ It belongs to the Krüppel-associated box (KRAB) Cys2His2 (C2H2)-type zinc finger proteins, which represent the largest individual family of transcription factors in the human proteome.¹⁵ Kaplan-Meier survival analysis based on the 99 patients showed that individuals with ZNF83 mutations (MUTs)

had a worse overall survival rate and cancer-specific survival rate compared to individuals with wild-type (WT) ZNF83 (Figures 1D and 1E, log-rank test, $p < 0.001$). The clinicopathological association study showed that ZNF83-MUT was significantly correlated with tobacco smoking ($p = 0.0215$) and clinical stage ($p = 0.0323$, Table 1). In a multivariate Cox regression analysis, ZNF83-MUT was further validated as an independent prognostic factor for the overall survival of UCs ($p = 0.0030$, Table 2). In total, we identified six recurrent somatic mutations, including a hotspot mutation encoding ZNF83-E293V that was found in 16.2% (16 of 99) of the UC cases. All of the missense mutation spots were dispersed throughout the C2H2-zinc finger domains, which exhibit sequence-specific DNA-binding functions (Figure 1F). Also, ZNF83-E293V was the most mutated site in other cancers analyzed by the HIVE biochemistry (Figure S1D). The phylogenetic analysis indicated that ZNF83 was evolutionarily well conserved. The alignment of ZNF83 across six different species revealed that amino acids were conserved in p.E293V analyzed by Clustal Omega (<https://www.ebi.ac.uk/Tools/msa/clustalo/>) (Figure 1G).

ZNF83-E293V Mutation Increased NF- κ B Activation Compared to ZNF83-WT in UC Cells

The KRAB C2H2-type zinc finger protein plays critical roles in a range of essential biological processes in cancer development.¹⁶ However, the role of ZNF83 in cancer has not been characterized. To investigate which signaling pathways are affected by the ZNF83-E293V mutation, we first evaluated the mutation status and expression levels of ZNF83 in one human urothelial immortalized cell line (SV-HUC-1 [SV]) and seven UC cell lines. We identified that the cells carried no ZNF83 mutation at the p.293 site by Sanger sequencing. UMUC-3 and 5637 cells harbored the lowest expressions of ZNF83 (Figures S2A–S2D). Then, ZNF83-WT and ZNF83-E293V mutant vectors (VECs) (Figure S3A) were cloned into lentivirus and successfully transfected into UMUC-3 and 5637 cells, respectively. Empty VEC-transfected UC cells (ZNF83-VEC) were used as negative controls (Figures S3B–S3E).

Next, we performed the gene set enrichment analysis (GSEA, <https://www.broadinstitute.org/gsea>) based on the The Cancer Genome Atlas (TCGA) bladder carcinoma (BLCA) data. We found that nuclear factor κ B (NF- κ B) pathway activation was negatively correlated with ZNF83-WT overexpression (Figure 2A). To investigate whether ZNF83-E293V mutation regulates the NF- κ B pathway, we selected some NF- κ B target genes for validation through qRT-PCR, as NF- κ B is a family of transcription factors that initiated the orchestration of inflammation. We found that the expression of seven NF- κ B target

Figure 1. ZNF83 Was Frequently Mutated and Correlated with Poor Prognosis in UC

(A) The mutation profile of genes with recurrent somatic mutations in the 99 subjects with UC. A different color in each bar represents different somatic alterations in the specified gene. The upper histogram shows the number and type of somatic mutations in each sample. (B) Sanger sequencing confirmation of ZNF83 somatic mutations identified from the genomic DNA in both tumors and corresponding non-tumorous bladder. Three individuals with four ZNF83 mutations are shown. The colors represent the four bases: green, A; blue, C; black, G; red, T. (C) Diagram summarizing the number of UC cases carrying the ZNF83 mutations in the discovery cohort (whole-genome and whole-exome sequence) and validation cohort (Sanger sequence). (D and E) Kaplan-Meier survival analysis showed that the ZNF83 mutation was significantly associated with unfavorable overall survival (D) and cancer-specific survival (E) in our cohort. (F) Schematic diagram showing the alterations of the amino acid changes in ZNF83 by the identified genetic changes. Zinc finger domains are highlighted in blue. The top two mutated positions, E293V and K290R, were located in the seventh Pfam zf-C2H2 domain. (G) Phylogenetic analysis of evolutionary relationships and multiple alignments of ZNF83 amino acid sequences among different species.

Table 1. Comparison of Clinical Characteristics between UC Patients with ZNF83-WT and ZNF83-MUT in 99 UC Patients

Variables	Total (Cases, %)	ZNF83-WT (%)	ZNF83-MUT (%)	p Value
Age group (years)				0.1650
<60	38 (38.4)	28 (28.3)	10 (10.1)	
≥60	61 (61.6)	53 (53.5)	8 (8.1)	
Sex				0.6784
Female	11 (11.1)	9 (9.1)	2 (2.0)	
Male	88 (88.9)	72 (72.7)	16 (16.2)	
Tobacco smoking				0.0215*
Smoker	50 (50.5)	36 (36.4)	14 (14.1)	
Non-smoker	49 (49.5)	45 (45.5)	4 (4.0)	
Family history of cancer				0.6638
Yes	21 (21.2)	16 (16.2)	5 (5.0)	
No	78 (78.8)	65 (65.7)	13 (13.1)	
Primary/relapsed				0.1504
Primary	86 (86.9)	68 (68.7)	18 (18.2)	
Relapsed	13 (13.1)	13 (13.1)	0 (0)	
Clinical stage				0.0323*
Stage I+II	58 (58.6)	52 (52.5)	6 (6.1)	
Stage III+IV	41 (41.4)	29 (29.3)	12 (12.1)	

*p < 0.05, **p < 0.01. The p value was calculated by a χ^2 test.

genes was elevated in ZNF83-E293V-transfected UMUC-3 cells as compared to the ZNF83-WT-transfected controls (Figure 2B). In addition, we observed that the expression of phosphorylated p65 and phosphorylated I κ B α were increased in ZNF83-E293V-transfected UMUC-3 and 5637 cells compared to ZNF83-WT controls (Figures 2C–2E). The immunofluorescence (IF) showed that the nuclear expression and distribution of phosphorylated p65 were inhibited by overexpression of ZNF83-WT and ZNF83-E293V, while ZNF83-E293V increased NF- κ B activation compared to ZNF83-WT in UC cells (Figures 2F–2H).

ZNF83-E293V Mutation Reduced the Transcriptional Repression of S100A8 Regulated by ZNF83-WT

To understand the underlying mechanism of ZNF83 regulation of the NF- κ B pathway, we performed RNA sequencing (RNA-seq) in UMUC-3 and 5637 cells stably transfected with empty VEC or ZNF83-WT and compared the differential transcriptome profiles. The overlaps of differentially regulated genes detected in both cell lines were selected for further analysis (Figure 3A). In comparison with the control groups, a total of 270 genes were differentially expressed by the overexpression of ZNF83 (Figure 3B). Because ZNF83 is a potential transcriptional repressor,¹⁵ we identified that S100A8 was the top downregulated gene by ZNF83 overexpression among the candidate target panels (Figure 3C). S100A8, also known as MRP8 or calgranulin A, was reported to contribute to inflamma-

Table 2. Univariate and Multivariate Overall Survival Analysis of Various Prognostic Parameters for UC Patients by Cox Proportional Hazard Model

Variables	Univariate Analysis		Multivariate Analysis	
	Hazard Ratio for OS (95% CI)	p Value	Hazard Ratio for OS (95% CI)	p Value
Age (<60 versus ≥60 years)	2.217 (1.071–4.590)	0.0320*	2.226 (1.045–4.741)	0.0380*
Sex (male versus female)	1.113 (0.391–3.169)	0.8410		
Tobacco smoking (smoker versus non-smoker)	0.800 (0.403–1.589)	0.0524		
Clinical stage (I+II versus III+IV)	1.751 (1.349–4.156)	0.0050**	1.920 (1.336–4.951)	0.0070**
ZNF83 mutation (MUT versus WT)	2.492 (2.022–5.979)	<0.001***	2.343 (1.788–6.097)	0.0030**

*p < 0.05, **p < 0.01, ***p < 0.001. OS, overall survival; CI, confidence interval.

tion-associated human neoplasia by increasing evidence.^{17,18} To investigate whether S100A8 is the targeted gene regulated by ZNF83, we first examined the association between the expression of S100A8 and ZNF83. We identified obvious inhibition of S100A8 at the mRNA as well as protein levels in ZNF83-WT-transfected UC cells compared to ZNF83-VEC groups (Figures 3D–3G). Since ZNF83 exerts its effects via binding to specific regions on the promoter of its target genes, the TRANSFAC database (<http://gene-regulation.com/pub/databases.html>) was applied to analyze potential ZNF83 binding sequences (ZBSs) on the promoter region of S100A8 (GenBank: NM_002964.4) (Figure 3H).

Two potential ZBSs were identified on the promoter of S100A8: ZBS1, consensus motif 5'-TGGCAACAACA-3', located at position –470, sense strand; and ZBS2, consensus motif 5'-TGTGAGAA-3', located at position –1820, sense strand. To test whether the identified ZBS motifs contribute to the inhibition of S100A8 promoters in response to ZNF83, we designed three promoter luciferase reporter constructs for the S100A8 promoter, containing the whole promoter sequence (A8-P1, –2058 to +150), upstream sequence containing ZBS2 (A8-P2, –2058 to –1620), or downstream sequence containing ZBS1 (A8-P3, –650 to –100), and analyzed the effect of ZNF83-WT and ZNF83-E293V on luciferase activity. The results showed that the activity of A8-P1, containing two potential ZBSs, dropped by 39% in ZNF83-WT-transfected cells, while this decline was 28% in ZNF83-E293V cells compared to the controls. A8-P2 activity was not inhibited by ZNF83-WT or ZNF83-E293V, suggesting that ZBS2 located at this region on the S100A8 promoter is not functional. However, the activity of A8-P3 containing only ZBS1 was attenuated 57% and 41% by ZNF83-WT and ZNF83-E293V, respectively (Figure 4A). We further explored the binding activity of ZNF83-WT and E293V on the S100A8 promoter in 5637, UMUC-3, and SV cells using a chromatin immunoprecipitation (ChIP)-quantitative real-time PCR assay. The

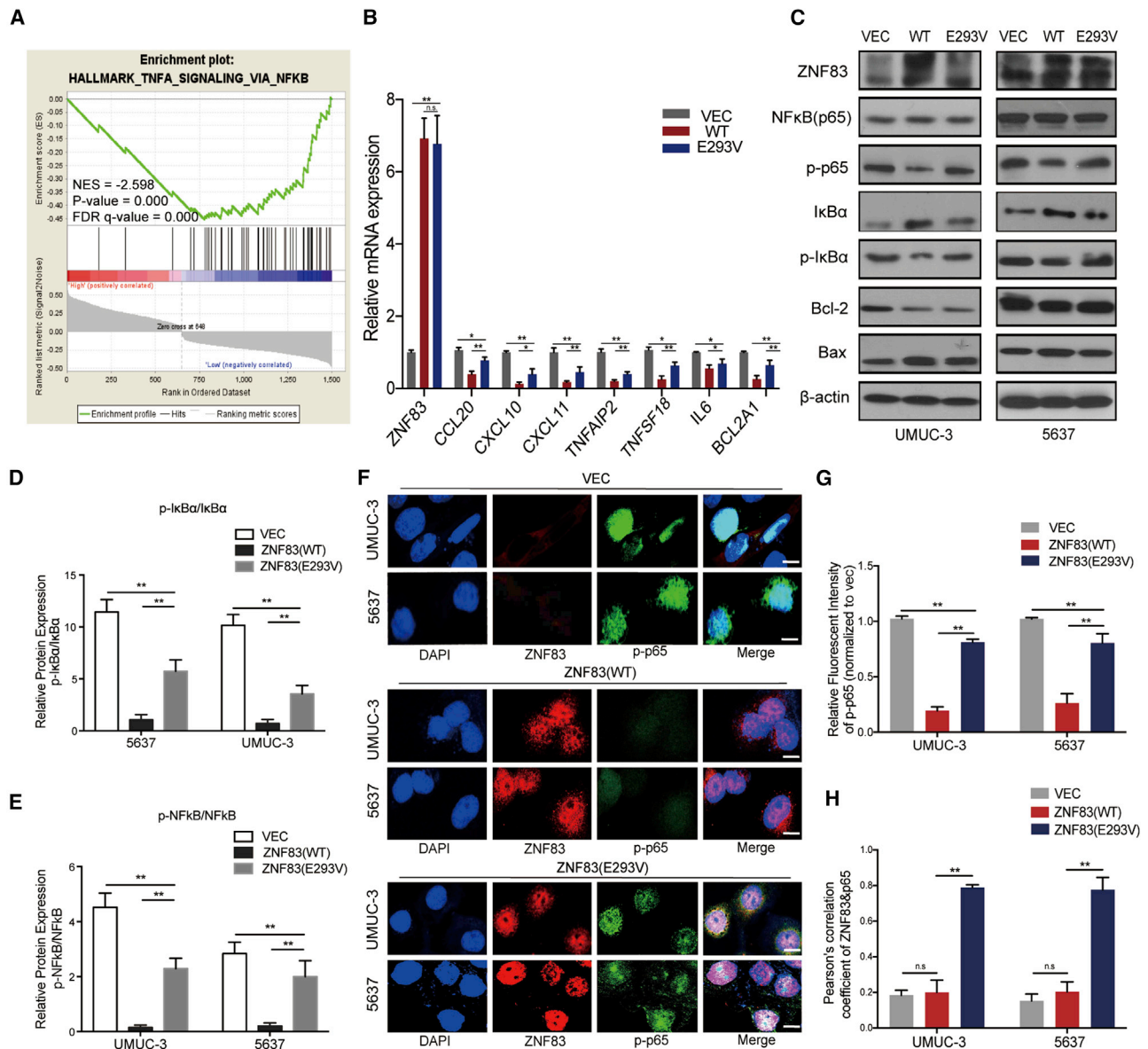


Figure 2. ZNF83-E293V Mutation Increased NF-κB Activation Compared to ZNF83-WT in UC cells

(A) GSEA of genes from TCGA RNA-seq data (BLCA) demonstrated that the NF-κB pathway negatively correlated with ZNF83 (WT) overexpression. The horizontal bar in graded color from red to blue shows the rank-ordered, non-redundant list of genes. The vertical black lines represent the projection of individual genes onto the ranked gene list. Genes on the right side (blue) correlated most strongly with increased NF-κB related gene expression. (B) Quantitative real-time PCR analysis of NF-κB target genes in ZNF83-VEC (VEC)-, ZNF83-WT (WT)-, or ZNF83-E293V (E293V)-transfected UMUC-3 and 5637 cells. Fold changes (FCs) relative to VEC-transfected cells in each group are shown. *p < 0.05, **p < 0.01, and n.s. not significant, tested by one-way ANOVA followed by Tukey's multiple comparison post hoc test. (C) Protein levels of NF-κB pathway genes in VEC-, WT-, or E293V-transfected UMUC-3 and 5637 cells detected by western blot. β-Actin was used as a loading control. (D and E) The ratio of relative protein expression of p-IκBα/IκBα (D) and p-NF-κB/NF-κB (E). Data are presented as means ± SD. **p < 0.01. (F) Immunofluorescence staining of p-p65 (green) and ZNF83 (red) in VEC-, WT- or E293V-transfected UMUC-3 and 5637 cells. Nuclei were identified using DAPI (blue). Scale bars, 20 μm. Data are representative of three independent experiments. (G) Quantitative analysis of the relative staining intensity of p-p65. The intensities were quantified by ImageJ software. Data are presented as means ± SD. **p < 0.01. (H) The levels of co-localization of p-p65 and ZNF83 assessed by Pearson correlation coefficient analysis on 10 sight fields in each group. Data are presented as means ± SD. **p < 0.01. n.s., not significant.

sequence details of ZNF83 binding site 1 and ChIP-quantitative real-time PCR primers on the S100A8 promoter are shown in Figure 4B. The results showed that S100A8 promoter fragments spanning ZBS1

were efficiently precipitated by FLAG antibody in ZNF83-WT and ZNF83-E293V-overexpressed cells compared to the immunoglobulin G (IgG) control, while the binding activity of ZNF83-E293V on the

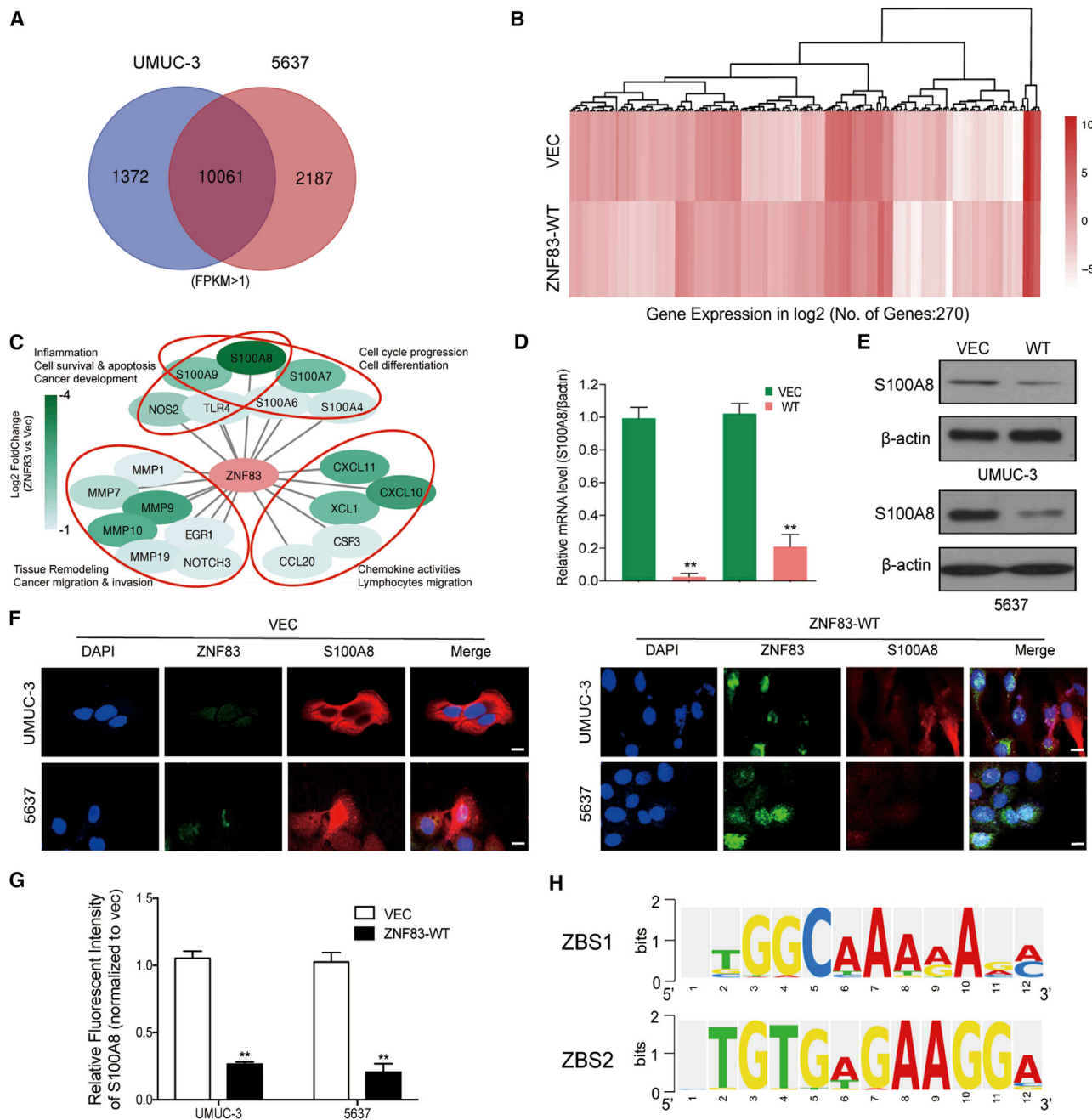


Figure 3. ZNF83-WT Repressed the Expression of S100A8 in UC Cells

(A) Whole-transcriptome analysis performed with RNA sequence in two pairs of UC cells UMUC3-WT versus UMUC3-VEC and 5637-WT versus 5637-VEC. The Venn diagram illustrates the overlap of differentially expressed genes with FPKM > 1. (B) Heatmap of significantly differentially expressed genes with p value < 0.01 and $\log_2(\text{FC})$ > 1 or less than -1. The results are presented as \log_2 FC values between the mean expression values of two sample groups. Color-coding is based on log-transformed read count values. (C) Panel of most downregulated genes by ZNF83 overexpression, in which S100A8 was the top downregulated gene. (D and E) Expression levels of S100A8 mRNA and protein were determined by quantitative real-time PCR (D) and western blot (E) in UMUC-3 and 5637 cells overexpressed with ZNF83-WT. (F) Representative immunofluorescence images of S100A8 (red) and ZNF83 (green) in VEC and ZNF83-WT overexpressed UMUC-3 and 5637 cells. Nuclei were counterstained with DAPI. Scale bars, 20 μm . (G) Quantitative analysis of the relative staining intensity of S100A8 in VEC and ZNF83-WT overexpressed cells. Data are presented as means \pm SD. ** p < 0.01. (H) Sequence logos of ZNF83-binding sites ZBS1 and ZBS2.

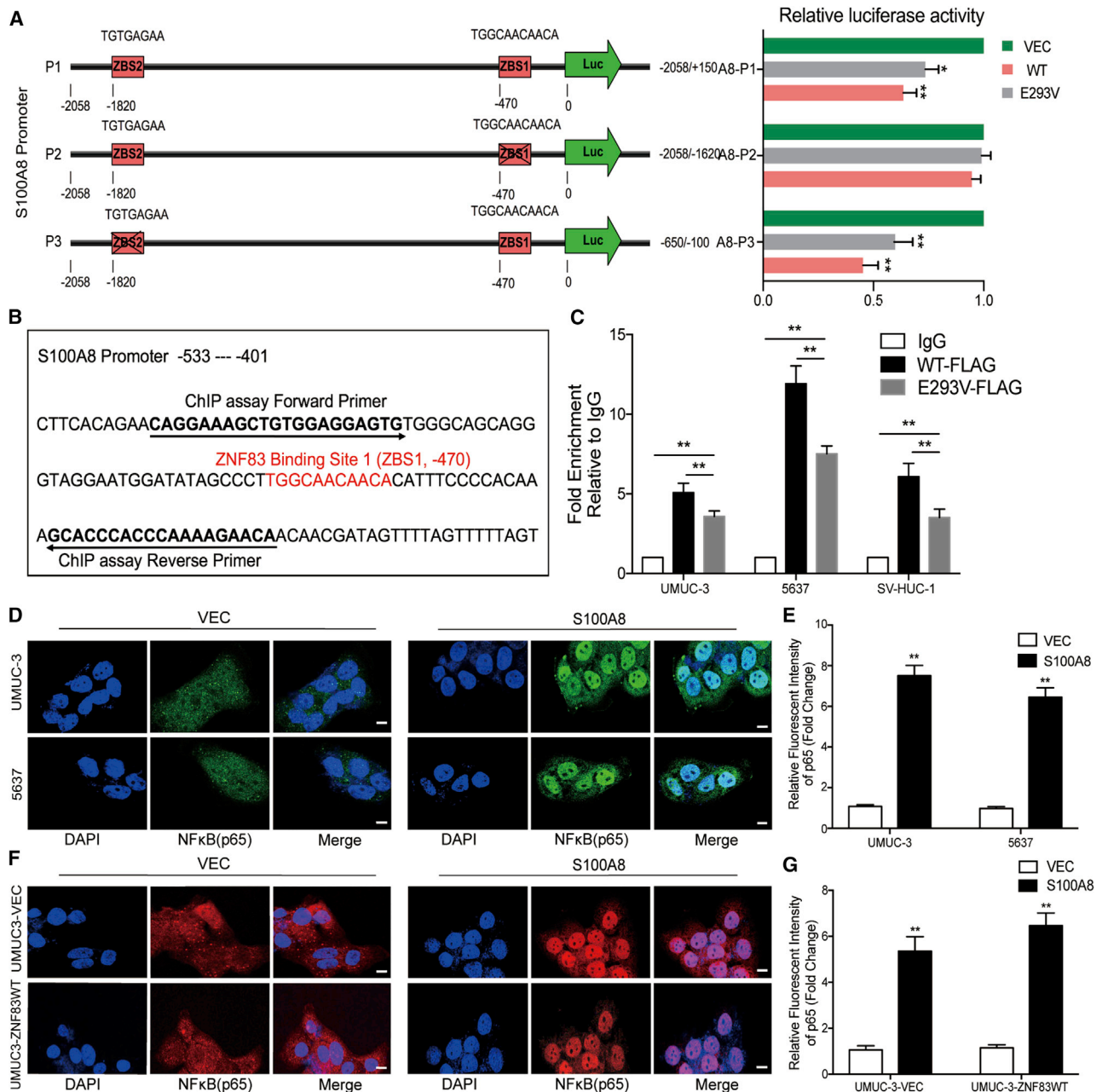
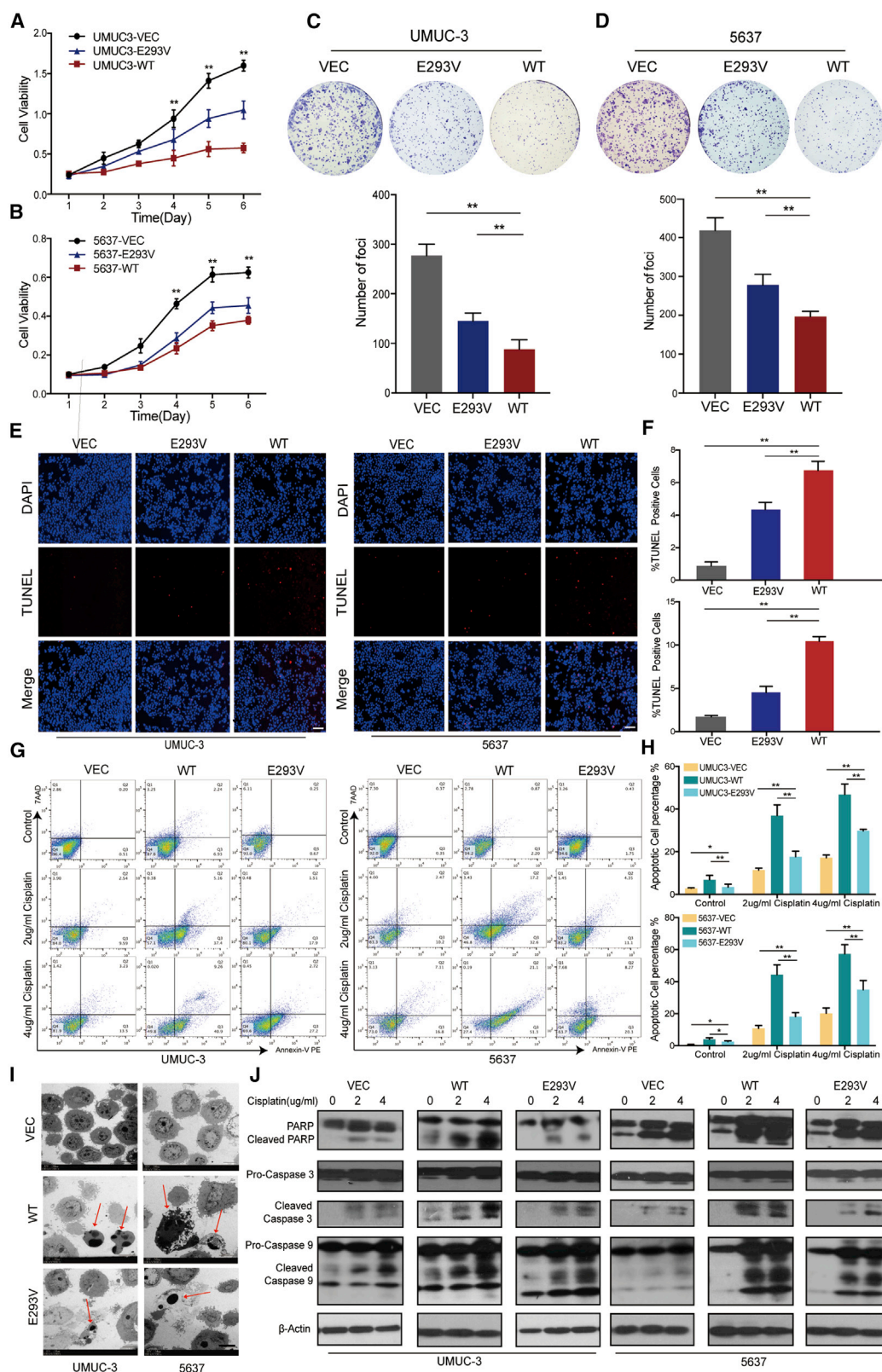


Figure 4. ZNF83-E293V Mutation Impaired the Transcriptional Repression of S100A8 in UC Cells

(A) Dual-luciferase reporter assay was used to detect the transcriptional regulation of ZNF83-WT and ZNF83-E293V on its targeted gene S100A8. The left panel shows two putative ZNF83-binding sites (ZBS1 and ZBS2) and their locations on the S100A8 promoter region, and the right panel shows the truncation analysis of the S100A8 reporters. (B) The sequence of ZNF83-binding site 1 (ZBS1) and the primer sequences of ChIP assay located on the S100A8 promoter. (C) FLAG-tagged ZNF83 (WT and E293V) were followed by a ChIP assay in UMUC-3, 5637, and SV-HUC-1 cells. Precipitated DNAs were quantified by quantitative real-time PCR for promoter regions of the S100A8 gene. The results are expressed as the mean \pm SD of triplicate samples. $**p < 0.01$. (D) Immunofluorescence staining of p65 (green) in VEC- or S100A8-transfected UMUC-3 and 5637 cells. Nuclei were stained blue. Scale bars, 20 μ m. (E) Quantitative analysis of the relative staining intensity of p65. The intensities were quantified by ImageJ software. Data are presented as means \pm SD. $**p < 0.01$. (F) The immunofluorescence staining of p65 (red) in VEC and ZNF83-WT overexpressed UMUC-3 cells treated with VEC or S100A8. Nuclei were stained blue. Scale bars, 20 μ m. (G) Analysis of the relative staining intensity of p65. Data are presented as means \pm SD. $**p < 0.01$.



(legend on next page)

S100A8 promoter was significantly lower than that of ZNF83-WT (Figure 4C). These results demonstrated that ZNF83-WT could directly bind to ZBS1 and mediate the inactivation of S100A8, thus attenuating the transcription of S100A8, whereas ZNF83-E293V mutation impaired its transcriptional-repressive ability.

Notably, inconsistent with previous studies, we identified that overexpression of the S100A8-encoding gene increased nuclear translocation of NF- κ B in 5637 and UMUC-3 cells (Figures 4D and 4E). Furthermore, in order to examine whether ZNF83-WT inhibited NF- κ B signaling in a S100A8-dependent manner, we transfected S100A8 and VEC to UMUC-3-ZNF83WT and UMUC-3-VEC cells. IF showed that NF- κ B was activated by overexpression of S100A8 in both UMUC-3-ZNF83WT and UMUC-3-VEC cells compared to VEC groups (Figures 4F and 4G). The results suggested that ZNF83-WT inhibited the NF- κ B pathway mainly via directly binding with the S100A8 promoter and inhibited its transcription, while ZNF83-E293V increased the activation of the NF- κ B pathway through the partial loss of transcriptional inhibition on S100A8.

ZNF83-E293V Mutation Increased the Proliferation and Decreased the Induced Apoptosis of UC Cells Compared to ZNF83-WT

Normally, NF- κ B activation in various human tumors results in transcription and expression of anti-apoptotic proteins, which contributes to tumor development.^{19–21} We next explored the consequences of ZNF83-E293V mutation-increased NF- κ B activation in UC. An XTT (2,3-bis-(2-methoxy-4-nitro-5-sulphophenyl)2*H*-tetrazolium-5-carboxanilide) assay and foci formation assays revealed that UMUC-3 and 5637 cells transfected with ZNF83-WT exhibited inhibition in tumor cell proliferation with respect to control groups. However, ZNF83-E293V showed significantly lower suppressive ability than did the ZNF83-WT cells ($p < 0.01$; Figures 5A–5D). In addition to increasing proliferation, we discovered that ZNF83-E293V mutation reduced the induced-apoptosis compared to ZNF83-WT in UC cells. A TUNEL (terminal deoxynucleotidyltransferase-mediated deoxyuridine triphosphate nick end labeling) assay showed that the pro-apoptotic effect of ZNF83-E293V was significantly lower than that of ZNF83-WT in UMUC-3 and 5637 cells after serum starvation for 24 h ($p < 0.01$; Figures 5E and 5F). To further confirm the effects of ZNF83 on cell apoptosis, ZNF83-WT-, ZNF83-E293V-, and ZNF83-VEC-transfected

UMUC-3 and 5637 cells were treated with 2 and 4 μ g/mL DDP for 48 h to induce apoptosis and examined using flow cytometry. The results showed that the apoptotic index induced by ZNF83-E293V was significantly lower than that of ZNF83-WT in both the 2 and 4 μ g/mL DDP treatment groups ($p < 0.01$; Figures 5G and 5H). Similar results were corroborated at the ultrastructural level by using transmission electron microscopy (TEM) examination in UMUC-3 and 5637 cells treated with serum-starvation for 24 h (Figure 5I). Western blot analysis further confirmed that ZNF83-WT was more potent at inducing the activation of apoptosis-associated proteins than ZNF83-E293V, which was reflected by the expression of cleaved poly(ADP-ribose) polymerase (PARP), caspase-9, and caspase-3 (Figure 5J).

ZNF83-E293V Mutation Increased Tumor Growth of UC in Mice Compared to ZNF83-WT

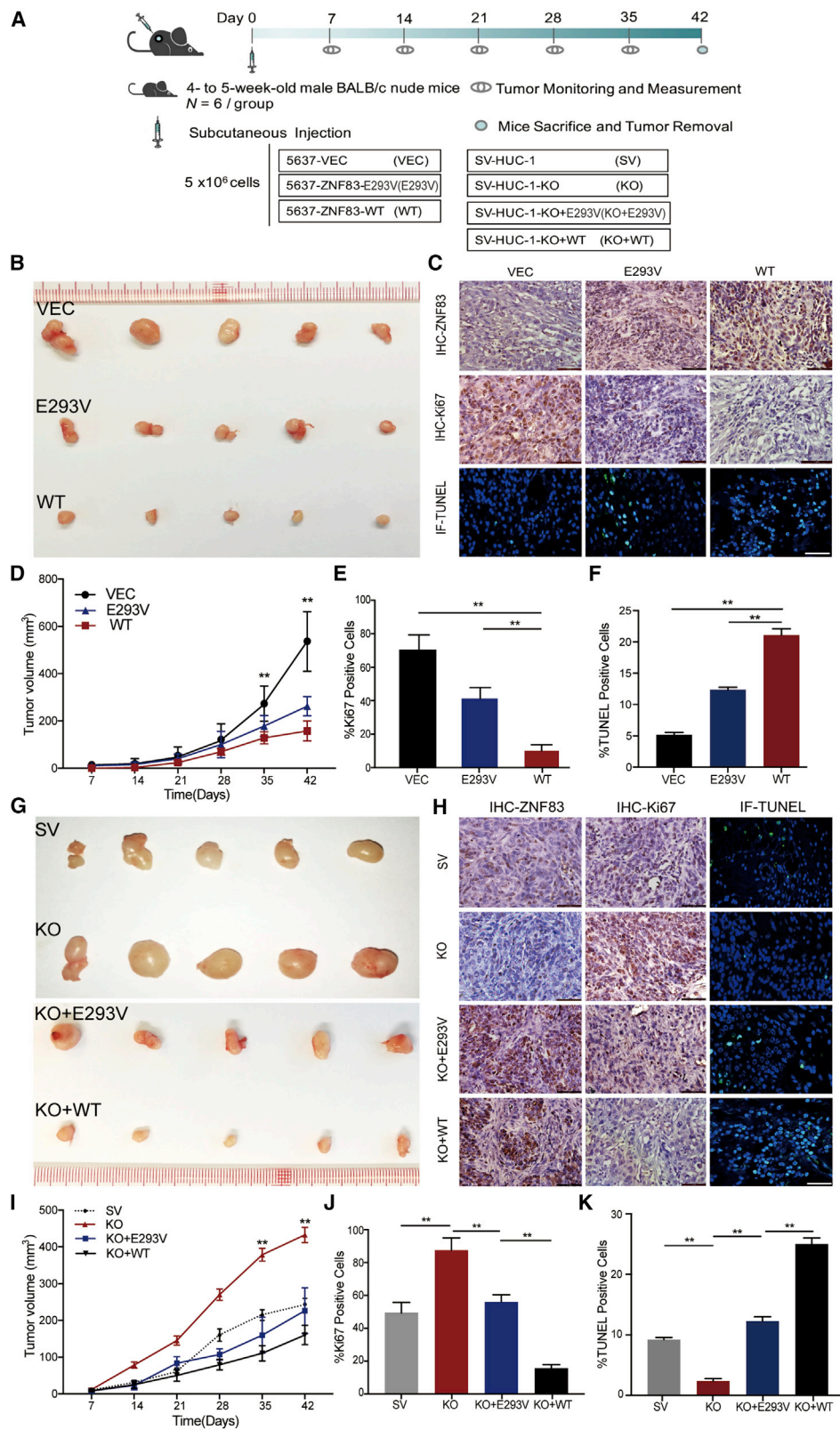
We then established xenograft mice models to test these findings *in vivo*. ZNF83-VEC-, ZNF83-E293V-, and ZNF83-WT-transfected 5637 cells were subcutaneously injected respectively into nude mice (Figure 6A). 6 weeks later, the tumor growth rates between these cells were distinguishable and the tumor volume and growth rate were significantly enhanced in tumors induced by ZNF83-E293V compared to those induced by ZNF83-WT ($p < 0.01$; Figures 6B and 6D). Moreover, the Ki67-positive frequencies in xenograft tumors induced by ZNF83-E293V were significantly higher than those induced by ZNF83-WT, and the TUNEL-positive cell rates in xenograft tumors induced by ZNF83-E293V were significantly lower than those induced by ZNF83-WT ($p < 0.01$; Figures 6C, 6E, and 6F).

In addition, we used the CRISPR-Cas9 system to knock out (KO) genomic ZNF83 completely in SV cells. First, we analyzed the karyotype of SV cells (Figure S4A) and then designed three guide RNAs (gRNAs) targeting the coding region of ZNF83 (Figure S4B). With the validation of efficiency and precision of targeted KO of ZNF83 in the mixed population of cells (Figures S4C–S4H), two single clones edited by single guide RNA (sgRNA)3 named KO (C2) and KO (C3) with complete ZNF83 KO were successfully isolated and validated (Figure S4I). We then selected KO (C3) cells for further animal experiments.

The *in vivo* results showed that, with the KO of ZNF83, the tumor growth rate induced by SV-KO cells was significantly enhanced.

Figure 5. ZNF83-E293V Mutation Increased Proliferation and Decreased Apoptosis of UC Cells Compared to ZNF83-WT

(A and B) Growth curves of VEC-, E293V-, and WT- transfected UMUC-3 (A) and 5637 (B) cells detected by an XTT cellular proliferation assay. Results are presented as mean \pm SD of three independent experiments. ** $p < 0.01$, tested by one-way ANOVA. (C and D) Representative images of foci formed by VEC-, E293V-, and WT- transfected UMUC-3 (C) and 5637 (D) cells in monolayer culture and relevant quantitative analysis of the number of foci and colonies. Results are presented as mean \pm SD of three independent experiments. ** $p < 0.01$, tested by one-way ANOVA followed by Tukey's multiple comparison post hoc test. (E) TUNEL assay of apoptotic cells (red signal) with cell nuclei counterstained with DAPI (blue signal) in UMUC-3 and 5637 cells. Scale bars, 100 μ m. (F) The apoptosis ratio was calculated by plotting the number of TUNEL-positive cells against that of DAPI-positive cells and summarized in the bar chart. The data represent the mean \pm SD of three independent experiments. ** $p < 0.01$, tested by one-way ANOVA with Tukey's post hoc test. (G) Cellular apoptosis induced by cisplatin at 2 and 4 μ g/mL concentrations was compared between VEC-, WT-, and E293V-transfected UMUC-3 and 5637 cells by flow cytometry analysis. Annexin V-stained positive cells were counted as apoptotic cells. (H) Quantitative analysis of the apoptosis ratio. Results are presented as mean \pm SD of three independent experiments. * $p < 0.05$, ** $p < 0.01$, tested by one-way ANOVA followed by Tukey's post hoc test. (I) Representative transmission electron microscopy (TEM) images of VEC-, WT-, and E293V-transfected UMUC-3 cells (top panel) and 5637 cells (bottom panel). The arrow depicts apoptotic cells and apoptotic bodies. Scale bars, 5 μ m. (J) Activation of apoptosis-associated proteins in VEC-, WT-, and E293V-transfected UMUC-3 and 5637 cells analyzed by western blot after treatment with different concentrations of cisplatin. β -Actin was used as a loading control.



(legend on next page)

Meanwhile, when ZNF83-WT and ZNF83-E293V were re-introduced in SV-KO cells (Figure S4F), the tumor-promoting effects induced by the silencing of ZNF83 could be rescued ($p < 0.01$, Figures 6G and 6I). The tumor growth and apoptosis differences among different groups were also revealed by the analysis of Ki67-positive frequencies and TUNEL-positive cell rates in xenograft tumors ($p < 0.01$; Figures 6H, 6J, and 6K). Thus, the results revealed that ZNF83-WT exhibited tumor suppressive ability in UC while the ZNF83-E293V mutation significantly increased tumor growth compared to ZNF83-WT. The results suggested that ZNF83 acted as a tumor suppressor gene and ZNF83-E293V is a loss-of-function mutation in UC.

Pharmacological Block of ZNF83-E293V-Induced Tumor Growth

On the basis of the above results, we next examined the possibility that drugs inhibiting NF- κ B activation might be beneficial in controlling ZNF83-E293V-induced UC tumor growth. Two potent NF- κ B inhibitors (caffeic acid phenethyl ester [CAPE] and dehydroxymethyl derivative of epoxyquinomicin [DHMEQ]) were selected for testing their efficiency in ZNF83-E293V-transfected 5637 cells. CAPE is an active component of propolis extract and specifically cause the inhibition of NF- κ B activity.²² DHMEQ acts by binding to a Cys residue of p65 to prevent nuclear translocation of p65.²³ The western blotting and IF validated that the nuclear localization of phosphorylated (p-) p65 was considerably decreased when treated at relatively high doses of drugs in 5637-ZNF83-E293V cells (5637-E293V), while the inhibition effects were not significant in 5637-ZNF83-WT cells (5637-WT) (Figures 7A–7C). An XTT assay showed that CAPE (10 μ M) and DHMEQ (10 μ g/mL) significantly inhibited the viability of 5637-E293V cells. However, these two drugs could not decrease the viability of 5637-WT cells significantly (Figure 7D). Also, cell clones were larger and more prevalent in the dimethyl sulfoxide (DMSO)-treated 5637-E293V cells, while the opposite results were observed in the drug-treated groups. For the 5637-WT cells, the number of foci exhibited no significant changes among different groups. The results indicated that the foci formation ability of 5637-E293V cells was significantly inhibited by CAPE (10 μ M) and DHMEQ (10 μ g/mL) (Figure 7E).

In order to test these findings in the xenograft mouse model, we treated nude mice, which were subcutaneously injected with 5637-

E293V and 5637-WT cells, with CAPE (10 mg/kg/day) and DHMEQ (10 mg/kg/day) (Figure 7F). The results showed that both of CAPE and DHMEQ suppressed the growth compared to the DMSO control group for 5637-E293V-induced tumors (Figures 7G and 7H). Also, between the two treatments, DHMEQ was more efficient in inhibiting tumor growth than was CAPE, demonstrating the efficacy of DHMEQ in suppressing ZNF83-E293V-induced tumor growth in a xenograft mouse model. Moreover, CAPE and DHMEQ increased the apoptosis of 5637-E293V-induced tumors compared to the control group (Figures 7I and 7J). In summary, our data revealed that compared to ZNF83-WT, ZNF83-E293V increased the transcription of S100A8 and NF- κ B pathway activation, which subsequently suppressed cell apoptosis and promoted cell survival, thus leading to UC progression.

DISCUSSION

It is well established that bladder cancer heterogeneity is significant and challenging. Genetic alterations in genes that encode proteins regulating critical aspects of cell survival and/or apoptosis play significant roles in bladder carcinogenesis.^{7,24} Different genetic studies on bladder tumors display overlaps, while remarkable differences distinguish them in alteration frequencies for specific genes.⁶ In this study, we reported a previously unappreciated mutated target, ZNF83, which was affected by somatic non-synonymous mutations in 18 of 99 (18%) UC patients. The validation experiments also supported the frequent mutation of ZNF83 in 3 of 33 (9.1%) UC patients. Of the 21 individuals, 17 carried ZNF83-E293V mutations. This somatic mutation hotspot was located in the seventh Pfam zf-C2H2 domain of ZNF83, which was evolutionarily highly conserved and took the essential DNA-binding function.

In addition, we analyzed ZNF83 mutation status in other studies by searching the cBioPortal based on TCGA data,¹² as shown in Figure 1B. In a whole-exome sequencing study from the United States, 4.17% of 72 UC cases had somatic mutations on ZNF83 in UC.²⁵ The frequency was lower than that in our study. The discrepancies between the studies might be explained by the distinct genetic backgrounds of Asian and Western populations, as germline variations could influence the somatic alterations in tumors.²⁶ Meanwhile, the mutation rates for ZNF83 vary extensively across cancer types. Gardner et al.²⁷ performed a whole-exome sequencing in 20 small-cell lung

Figure 6. ZNF83-E293V Mutation Increased Tumor Growth in Xenograft Mice Model Compared to ZNF83-WT

(A) Schematic of the xenograft mouse model. (B) Representative photographs of the subcutaneous tumors formed in nude mice following injection of 5637-VEC, 5637-ZNF83-E293V, and ZNF83-WT cells. (C) Representative IHC staining of sectioned xenograft tumors with anti-ZNF83 and anti-Ki67 antibody and immunofluorescent TUNEL-stained fixed tumor tissue sections. Positive staining is depicted in green. Nuclei were stained with DAPI. Scale bars, 100 μ m. (D) Tumor growth curves in 5637-VEC, 5637-ZNF83-E293V, and ZNF83-WT groups summarized in the line chart. The average tumor volume at each time point is expressed as the mean \pm SD of six mice. ** $p < 0.01$, tested by one-way ANOVA. (E and F) Percentage of Ki67 (E) and TUNEL (F) positively stained cells of xenograft tissues in 5637-VEC, 5637-ZNF83-E293V, and ZNF83-WT groups. Data are expressed as the mean \pm SD. ** $p < 0.01$, one-way ANOVA followed by Tukey's post hoc test. (G) Representative photographs of the subcutaneous tumors formed in nude mice following injection of SV-HUC-1, SV-HUC-1-KO, SV-HUC-1-KO+E293V, and SV-HUC-1-KO+WT cells. (H) IHC staining of sectioned xenograft tumors with anti-ZNF83 and anti-Ki67 antibody and immunofluorescent TUNEL-stained fixed tumor tissue sections in each group. Positive staining is depicted in green. Nuclei were stained with DAPI. Scale bars, 100 μ m. (I) Tumor growth curves in each group summarized in the line chart. The average tumor volume at each time point was expressed as the mean \pm SD of six mice. ** $p < 0.01$, tested by one-way ANOVA. (J and K) Percentage of Ki67 (J) and TUNEL (K) positively stained cells of xenograft tissues in each group. Data are expressed as the mean \pm SD. ** $p < 0.01$, one-way ANOVA followed by Tukey's post hoc test.

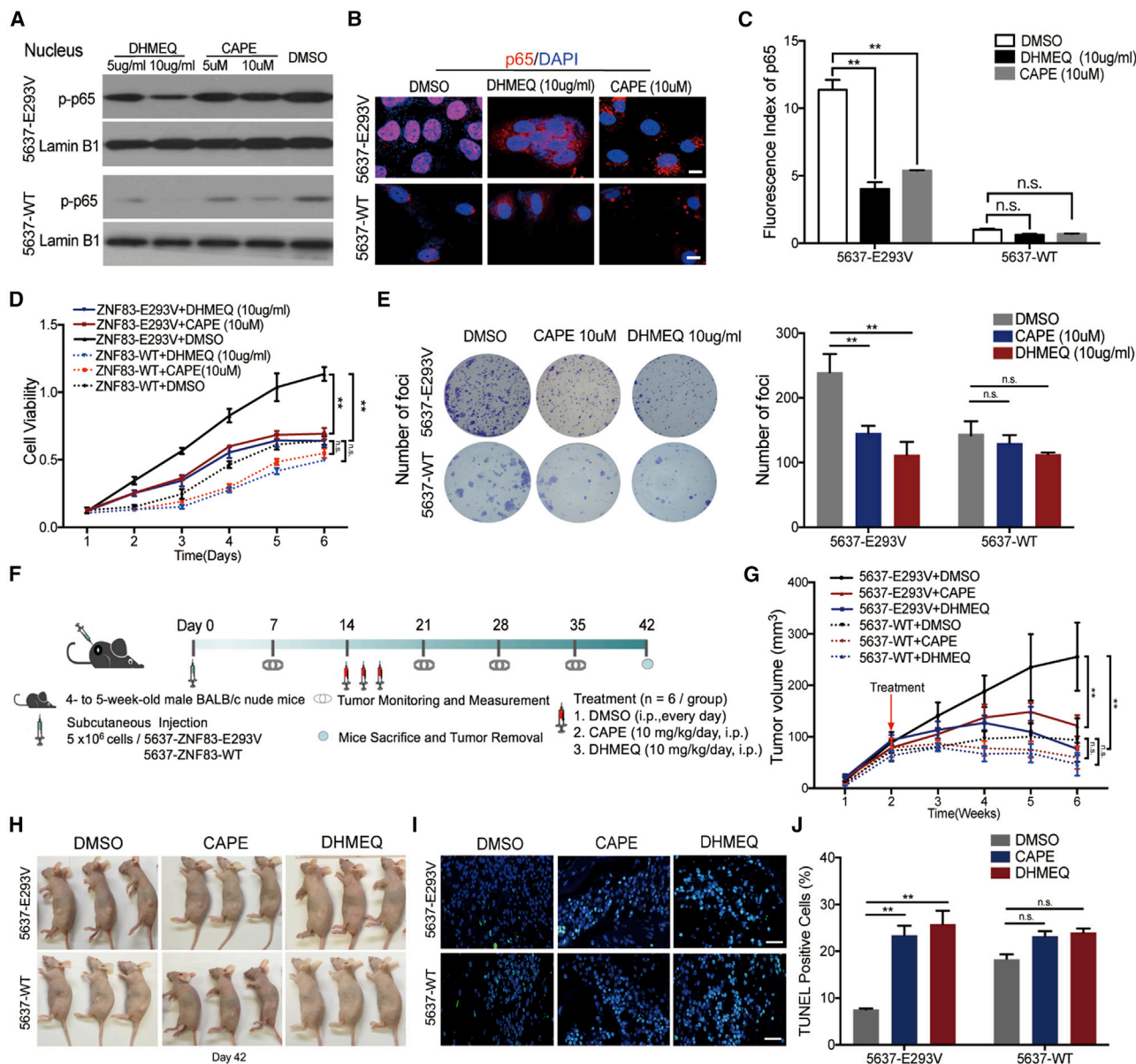


Figure 7. CAPE and DHMEQ Treatment Inhibited ZNF83-E293V-Induced UC Tumor Growth in Mice

(A) Analysis of the effects of CAPE and DHMEQ on NF- κ B activity in ZNF83-E293V- and ZNF83-WT-transfected 5637 cells. Western blotting of p-NF- κ B/p-p65 using proteins extracted from ZNF83-E293V- and ZNF83-WT-transfected 5637 cells cultured with DMSO, CAPE (10 μ M), CAPE (5 μ M), DHMEQ (10 μ g/mL), and DHMEQ (5 μ g/mL) for 24 h. Separate nuclear proteins were immunoblotted for p-p65. Lamin B1 served as a loading control. (B) Localization of NF- κ B/p65 analyzed by immunofluorescence in 5637-E293V and 5637-WT cells treated with DMSO, CAPE (10 μ M) or DHMEQ (10 μ g/mL). Scale bars, 20 μ m. (C) Statistical analysis of p65 fluorescence in each group. ** $p < 0.01$. n.s., not significant. (D and E) 5637-E293V and 5637-WT cells treated with DMSO, CAPE (10 μ M), or DHMEQ (10 μ g/mL) were seeded for XTT (D) and foci formation (E) assays. Each value represents the mean \pm SD from three independent experiments. ** $p < 0.01$, one-way ANOVA followed by Tukey's post hoc test. (F) The schematic of the *in vivo* study design. (G) Analysis of tumor growth from week 1 to week 6. The value represents mean \pm SD from triplicate experiments. ** $p < 0.01$, one-way ANOVA test. (H) Representative images of the mice and tumors on day 42. (I) Immunofluorescent TUNEL staining of sectioned xenograft tumors in each group. Positive staining is depicted in green. Nuclei were stained with DAPI. Scale bars, 100 μ m. (J) Analysis of TUNEL positively stained cells as percentage of xenograft tissues in each group. Data are expressed as the mean \pm SD. ** $p < 0.01$, one-way ANOVA followed by Tukey's post hoc test.

cancer samples and found that 45% of cases had in-frame deletion mutations (p.H271_F298del) in the ZNF83 gene. In another massively parallel sequencing analysis of uterine carcinosarcoma,

ZNF83 was found to harbor missense mutations (p.E84D and R281I) in 9.09% of all cases.²⁸ Interestingly, the mutated sites of ZNF83 in these two studies also involved the seventh Pfam zf-

C2H2 domain. This domain has also been reported to be pervasively mutated among other zinc finger proteins,^{11,29} suggesting the critical function of this residue. However, few studies have explored the biological function of ZNF83 and the impact of its mutation on tumorigenesis. To our knowledge, this is the first time to report the tumor suppressive role of ZNF83 in UC and the loss-of-function ZNF83-E293V mutation, which results in the pathogenesis of UC.

Clinically, the gold standard for MIBC is radical cystectomy with extended pelvic lymph node dissection, with or without chemotherapy. However, the 5-year recurrence-free survival in post-operative patients was only 34%–43%.³⁰ Increasing numbers of studies have reported on biomarkers that can be used as treatment targets or to identify patients who might benefit from more aggressive therapy.³¹ For instance, the emergence of FGFR3-directed targeted therapy brought hope to progressive UC patients.¹⁰ Also, some studies have implicated the use of NF- κ B as a potential therapeutic target in bladder cancer.³²

Generally, NF- κ B could be activated, for example, by infections, inflammatory cytokines, and irradiation. In this study, we found that the ZNF83-E293V mutation could activate NF- κ B signaling compared to ZNF83-WT, resulting in UC progression. This initial observation might have translational potential because we also found that the inhibitors of NF- κ B could significantly suppress the ZNF83-E293V-mediated tumor growth in mice model. These results indicated the potential use of ZNF83-E293V mutation as a predictor of therapeutic response from NF- κ B inhibitors. In addition, we found that ZNF83 mutation was associated with worse overall survival in our cohort. However, these preliminary results were far from sufficient to support ZNF83 mutation as a prognosis predictor or therapeutic target for UC. Further study with a larger cohort to clarify the potential clinical value of ZNF83 mutation in UC is needed.

Above all, the present study identified a tumor suppressor gene, ZNF83, and revealed the somatic mutation ZNF83-E293V, which contributed to the progression of UC. Our data further established a foundation for adopting NF- κ B inhibitors as putative therapeutics for precision therapy of ZNF83-E293V-mutated UC patients, which might provide a marker for UC management. Additionally, whether the combination of ZNF83 mutation with other effective gene signatures and clinical nomograms could be used for estimating long-term survival is also worth further investigation.

MATERIALS AND METHODS

Patients and Specimens

For the discovery cohort, 99 tumor samples with paired normal tissues were obtained from individuals diagnosed with UC (2010–2013) and underwent transurethral resection with partial or radical cystectomy without preoperative radiotherapy or chemotherapy at the member institutions of the Urinogenital Cancer Genomics Consortium (UCGC) in China. Clinical information in detail for each patient is as described previously.⁹ The statistical analysis of the baseline information is presented in Table 1. Clinical follow-up information was updated in 2019. For the validation cohort, 33 FFPE samples of

UC with paired normal tissues (2016–2018) were collected from Sun Yat-Sen University Cancer Center (Guangzhou, China). None of the patients received preoperative treatment. Clinical information is described in Table S3. Each patient was properly informed, and the study was approved by the Institutional Ethics Review Boards. All procedures involving human participants were in accordance with the 1964 Declaration of Helsinki.

Discovery and Validation of ZNF83 Mutations in UC

Analysis of significantly mutated genes in the discovery cohort was as described before.⁹ Briefly, the number of available nucleotides for each category was the total number of sufficiently covered (15 \times) bases for that particular category in all samples. The genes showing significantly higher mutation rates than background rates and harboring mutations in at least 5 of the 99 tumors were considered to be significantly mutated. For validation of ZNF83 mutations, we designed primers that uniquely amplify the CDS region of ZNF83 (Table S4) using Primer5.0 (Premier Biosoft). Genomic DNA from FFPE samples of 30 additional individuals with UC was extracted using the QIAamp DNA FFPE tissue kit (QIAGEN). PCR products were sent for Sanger sequencing and analyzed. All sequences were analyzed with sequencing analysis software.

Cell Lines and Reagents

Seven bladder cancer cell lines, that is, 5637 (ATCC HTB9), T24 (ATCC HTB4), RT-4 (ATCC HTB2), SW780 (ATCC CRL2169), HT-1376 (ATCC CRL1472), TCCSUP (ATCC HTB5), and UMUC-3 (ATCC CRL1749), and one human ureter uroepithelial cell line SV (ATCC CRL9520) were used in this study. All cell lines were purchased commercially from ATCC (Manassas, VA, USA) and maintained in RPMI 1640, F12K, or Dulbecco's modified Eagle's medium (Gibco-BRL, Grand Island, NY, USA) supplemented with 10% fetal bovine serum and 1% 200 mM L-glutamine (Kyowa Hakko Bio, Tokyo, Japan) at 37°C. The NF- κ B inhibitors CAPE and DHMEQ were purchased from Selleck Chemicals and MedChemExpress, respectively. CAPE and DHMEQ were dissolved in DMSO.

CRISPR-Cas9 Assay

Knockout of ZNF83 in UC cells was achieved by introducing a frame-shift mutation in ZNF83 guided by gene-specific gRNAs and cut by CRISPR-Cas9. Three gRNAs targeting the first 500 bp of exon 6 for ZNF83 (the coding sequences and common exon for all splice variants) were designed using freely available online tools.³³ The gRNA and the protospacer-adjacent motif (PAM) sequences are listed in Figure 3A. Then, the annealed oligonucleotides were ligated into the CRISPR-CAS9 VEC pLV-U6-sgRNA-cytomegalovirus (CMV)-hCas9-2A-EGFP (purchased from SyngenTech, China). All plasmids were sequenced to confirm successful ligation. SV cells (1 \times 10⁶) were plated overnight and transfected with CRISPR-Cas9 plasmids using Lipofectamine 2000 (Thermo Fisher Scientific, USA) and then selected by fluorescence-activated cell sorting (FACS Aria SORP, BD Biosciences). The sorted cells as well as the selected single-cell colonies were expanded. DNA was extracted for the mismatch-specific T7 endonuclease I (T7E1) validation and confirmed by Sanger sequencing. Protein extraction was used for western blotting.

Metaphase Spread Analysis

For karyotyping, SW780 and SV cells were treated with colcemid (Sigma-Aldrich, USA), and metaphase chromosome spreads were prepared on slides according to standard procedures. The slides were then counterstained with DAPI and observed under fluorescence microscopy (Leitz DMRB; Leica, Rueil-Malmaison, France).

T7E1 Cleavage Assay

The genomic DNA of SV cells was extracted using a DNA extraction kit (Tiangen, China). The genomic regions surrounding each target site were amplified using PrimerStar DNA polymerase (Takara, China) with the specific Cas9 validation primers listed in Table S4 and then purified following the manufacturer's protocol. T7E1 nuclease (GeneCopoeia, USA) was used to treat the mixture of duplexes. The reaction was stopped and the products were analyzed on a 2% agarose gel. Then, the PCR products with mutations detected by the T7E1 cleavage assays were chosen for validation by Sanger sequencing.

RT-PCR and Quantitative Real-Time PCR

Reverse transcription of total RNA was performed using the PrimeScript RT-PCR kit (Takara, Dalian, China). RT-PCR and quantitative real-time PCR were performed as per the standard procedures with a PCR amplification kit (Takara, Dalian, China) and FastStart SYBR Green master mix on an HT7900 system (Roche Applied Science, Penzberg, Germany), respectively. Primers used are listed in Table S4.

Western Blot

Western blot analyses were performed using standard methods. Briefly, total protein was isolated from treated cells, which were lysed in the radioimmunoprecipitation assay (RIPA) buffer containing protease inhibitors (Roche) and phosphatase inhibitors (Sigma). Denatured proteins were separated by SDS-PAGE and transferred onto a polyvinylidene fluoride (PVDF) membrane (Bio-Rad). Each protein was probed with specific primary antibodies and then with secondary antibodies (Table S5).

IF

Cells were seeded in chamber slides overnight and then fixed, permeabilized, blocked, and then incubated with primary antibodies at 4°C overnight and with secondary antibodies for 1 h at room temperature. The nucleus was stained by DAPI (Invitrogen, CA, USA). IF images were visualized under a Carl Zeiss LSM700 fluorescence microscope (Zeiss, Germany) and analyzed with ImageJ software.

In Vitro Tumorigenic Assays

An XTT cell proliferation assay was performed. Cells were seeded in 96-well plates at a density of 1×10^3 cells per well. The cell growth rate was measured using a cell proliferation XTT kit (Roche Applied Science, Germany) according to the manufacturer's instruction. Anchorage-dependent growth was assessed by a foci formation assay. 1×10^3 cells were seeded in a six-well plate. After 7 days of culture, colonies (>50 cells per colony) were stained and counted with crystal violet staining (Sigma-Aldrich, USA). Independent experiments were performed in triplicate.

TUNEL Assay

Apoptotic effects were determined by a TUNEL assay. Cells were fixed with formaldehyde and washed with PBS. Apoptotic cells were determined using an *In Situ* Cell Death Detection Kit, TMR red (Roche, USA), which quantitatively determines DNA fragmentation following the manufacturer's protocol. Apoptotic indices were obtained by counting the percentage of TUNEL-positive cells.

TEM

Apoptosis was also confirmed by TEM examination. Briefly, the indicated cells were gently harvested and fixed in 3% glutaraldehyde. The sections were treated with osmium oxide, dehydrated in alcohol, infiltrated with acetone, and then embedded and polymerized. 70- to 100-nm ultrathin sections were prepared, placed onto grids, and stained using uranyl citrate. Prepared samples were examined under a transmission electron microscope (Philips CM 100) and imaged.

Flow Cytometry

1×10^6 cells per well were plated in six-well plates. The anti-cancer drug cisplatin (2 or 4 $\mu\text{g}/\text{mL}$) was added to trigger apoptosis. After 48 h of incubation, cells were collected and dual-stained with annexin V-phycoerythrin (PE) and 7-aminoactinomycin D (7AAD) as provided by the PE annexin V apoptosis detection kit (BD Biosciences, CA, USA) according to the manufacturer's instructions. Analysis was determined by the FACSCanto II flow cytometer (Becton Dickinson, MA, USA).

RNA-Seq

RNA-seq analysis for UC cell lines UMUC-3 and 5637 stably transfected with ZNF83 and control VEC was performed using the Illumina HiSeq 2500 system (Illumina, San Diego, CA, USA) at Novogene Bioinformatics Technology (Beijing, China). Total RNA was isolated using TRIzol reagent (Thermo Fisher Scientific) according to the manufacturer's standard protocol, followed by the evaluation of RNA purity and concentration. The raw sequencing data were subjected to quality control to obtain clean data. The reads were aligned against the human reference genome (hg19) and normalized as FPKM (fragments per kilobase of transcript per million mapped reads). Transcripts with FPKM values <1 were removed. The remaining transcripts were used to perform the downstream analysis. Differentially regulated genes detected in both cell lines were selected for further analysis. Differential expression analysis was performed using the DEGseq (2010) R package and edgeR program package. The adjusted p value <0.05 and $|\log_2(\text{fold change})| >1$ were set as the thresholds for significant differential expression.

Dual-Luciferase Reporter Assay

To examine the transcriptional regulation of ZNF83 on the targeted genes, S100A8 promoter luciferase assays were performed as per the standard protocol. Briefly, fragments of various truncated promoter regions in S100A8 were inserted upstream of firefly luciferase coding sequences in the pGL3-enhancer reporter plasmid (Promega, USA). 5637 cells (1×10^4 cells/well) were seeded in 96-well plates in triplicate and incubated for 24 h. Then, the cells were transfected with

pGL3-enhancer (negative control), pGL3-ctrl (positive control), and pGL3-S100A8 promoter fragments, together with the Renilla luciferase reporter VEC. After 48 h of transfection, firefly luciferase and Renilla luciferase signals were determined using the Dual-Luciferase reporter assay kit (Promega, USA). Luciferase intensities of each well were normalized to the activities of Renilla luciferase. All experiments were performed three times for confirmation.

ChIP Assay

The ChIP assay was performed using a ChIP assay kit (Millipore, Billerica MA, USA, #17-295). FLAG-tagged ZNF83 lentivirus-transfected 5637 cells were seeded into a 10-cm dish and grown to 80% of confluency. 270 μ L of 37% formaldehyde was added to 10 mL of medium to crosslink the protein-DNA interaction. After washing three times with ice-cold PBS with protease inhibitor (PI), cells were scraped into a 1.5-mL tube. The cell pellet was lysed and sonicated to shear DNA to lengths between 200 and 500 bp. The lysates were cleared by centrifugation and diluted 10-fold into ChIP dilution buffer with PI. The supernatant fraction was incubated overnight with rotation at 4°C with 5 μ L of anti-FLAG M2 antibody (Cell Signaling Technology, #14793) and the same amount of normal mouse IgG (sc-2025, Santa Cruz Biotechnology, USA) as a negative control. Chromatin was cleared and incubated with protein A agarose beads for 1 h at 4°C. Beads were washed with high-salt, low-salt, and LiCl buffer. Immunoprecipitated DNA was recovered by incubation in 1% SDS and 100 mM NaHCO₃ for 30 min at room temperature (RT). Cross-linking was reversed by addition of NaCl (0.5 M) and incubation at 65°C for 4 h. Eluted DNA fragments were purified and analyzed by quantitative real-time PCR using SYBR Green in the ABI 7900HT fast real-time PCR system (Applied Biosystems). Primer sequences are listed in Table S4. Fold enrichment was calculated based on Ct as $2^{-\Delta\Delta Ct}$, where $\Delta Ct = Ct_{IP} - Ct_{Input}$ and $\Delta\Delta Ct = \Delta Ct_{FLAG\ antibody} - \Delta Ct_{IgG}$.

Animals

The animal experiments were performed under HK Animals Ordinance license (no. of license: 16-990 in DH/HA & P/8/2/3 Pt.91) according to standard policies. The experimental protocol was approved by the University of Hong Kong Animal Welfare Committee (approval no. CULATR-4090-16). All procedures were made to minimize the suffering and number of animals in compliance with the ethical standards of the institutional or national research committee. All animals used in this study were ordered from the Laboratory Animal Unit of the University of Hong Kong. All mice were kept in standard cages at 26°C \pm 1°C under a 12-h light/12-h dark cycle and fed the rodent standard diet with free access to water. The mice were randomly divided into control groups or experimental groups, with each group containing six mice. The *in vivo* tumorigenic ability of ZNF83 was investigated in 4- to 5-week-old male BALB/c nude mice (mean body weight, 15.5 \pm 1.2 g). Briefly, cells were suspended in sterile PBS and subcutaneously injected into the left dorsal flanks of nude mice. Then, tumor size was measured weekly after injection. Tumor volume was calculated by the formula $V = 0.5 \times L \times W^2$, where L is the length (long axis) and W is the width (short axis) of the tumors. After continued observation for 6 weeks, mice were

ethanized and tumors were collected for further pathological studies. For the pharmacological block study, the nude mice were adapted to the environment for 1 week, and 5×10^6 5637-E293V cells were re-suspended in 200 μ L of PBS and injected into each mouse subcutaneously. Treatment began when the tumor volume reached approximately 100 mm³ at 2 weeks after tumor cell injection. Xenograft mice were administered drugs by intraperitoneal injection. The xenograft mice were randomly divided into the three groups as follows: (1) the xenograft mouse group was treated with 2% DMSO; (2) the CAPE group was treated with CAPE at a dose of 10 mg/kg/day; and (3) the DHMEQ groups was treated with DHMEQ at a dose of 10 mg/kg/day. After treatment for 4 weeks, the mice were sacrificed, and tumors were removed and measured.

Immunohistochemistry (IHC)

IHC procedures and scoring of protein expression were performed according to the standard protocol. Briefly, sections were deparaffinized with xylene and rehydrated prior to antigen retrieval. Then, the slides were incubated with primary antibodies ZNF83 (1:200 dilution, Sigma-Aldrich, USA) and Ki67 (1:200 dilution, Abcam, USA) at 4°C overnight. The sections were then incubated with a secondary antibody (1:100 dilution, Santa Cruz, USA) for 30 min at room temperature. Finally, the 3,5'-diaminobenzidine substrate kit (Dako, Carpinteria, CA, USA) was used for signal development followed by Mayer's hematoxylin counterstaining. The positive expression percentages of ZNF83 and Ki67 were calculated by two independent pathologists.

Statistical Analysis

IBM SPSS Statistics 19 software (SPSS, Chicago, IL, USA) was applied to perform statistical analysis. The Kaplan-Meier plot and log-rank test were used for survival analysis. The one-way analysis of variance (ANOVA) followed by Tukey's multiple comparison post hoc test was used to determine the significant differences between two or more independent groups. The data are presented as the mean \pm standard deviation (SD) of three independent experiments. p values are denoted as *p < 0.05 and **p < 0.01 in all figures.

SUPPLEMENTAL INFORMATION

Supplemental Information can be found online at <https://doi.org/10.1016/j.ymthe.2020.09.004>.

AUTHOR CONTRIBUTIONS

X.Y.G. and Z.M.C. designed the study; X.Y.G. funded and supervised the molecular analysis; Z.J.L., Y.W., J.L.H., and C.J. performed *in vitro* analyses and analyzed the data; Z.J.L., Q.Y., and M.C. performed *in vivo* analyses; S.Y.W. and Y.Z. analyzed the data; Y.T., L.L., Y.C.C., and X.L. analyzed tissue stains; Y.Z.J. and Y.C.L. performed the biologic informatics analysis; H.B.M., F.W., and R.H.L. analyzed the clinical information; and Z.J.L. and Y.W. wrote the manuscript.

CONFLICTS OF INTEREST

The authors declare no competing interests.

ACKNOWLEDGMENTS

This work was supported by Hong Kong RGC grants, including GRF (767313) and Collaborative Research Funds (C7065-18GF); the National Natural Science Foundation of China (82073182, 81602421 and 81772554); the National Key R&D Program of China (2017YFC1309000); the Shenzhen Fundamental Research Program, China (grant no. JCYJ20180508153249223), and the Shenzhen Science and Technology Program, China (KQTD20180411185028798 and KQTD2015033117210153). X.Y.G. is a Sophie Y.M. Chan Professor in Cancer Research.

REFERENCES

- Hanahan, D., and Weinberg, R.A. (2011). Hallmarks of cancer: the next generation. *Cell* 144, 646–674.
- Cancer Genome Atlas Research Network (2014). Comprehensive molecular characterization of urothelial bladder carcinoma. *Nature* 507, 315–322.
- Antoni, S., Ferlay, J., Soerjomataram, I., Znaor, A., Jemal, A., and Bray, F. (2017). Bladder cancer incidence and mortality: a global overview and recent trends. *Eur. Urol.* 71, 96–108.
- Kamat, A.M., Hahn, N.M., Efstathiou, J.A., Lerner, S.P., Malmström, P.U., Choi, W., Guo, C.C., Lotan, Y., and Kassouf, W. (2016). Bladder cancer. *Lancet* 388, 2796–2810.
- Bray, F., Ferlay, J., Soerjomataram, I., Siegel, R.L., Torre, L.A., and Jemal, A. (2018). Global cancer statistics 2018: GLOBOCAN estimates of incidence and mortality worldwide for 36 cancers in 185 countries. *CA Cancer J. Clin.* 68, 394–424.
- Warrick, J.I., Sjödhall, G., Kaag, M., Raman, J.D., Merrill, S., Shuman, L., Chen, G., Walter, V., and DeGraff, D.J. (2019). Intratumoral heterogeneity of bladder cancer by molecular subtypes and histologic variants. *Eur. Urol.* 75, 18–22.
- Zhang, X., and Zhang, Y. (2015). Bladder cancer and genetic mutations. *Cell Biochem. Biophys.* 73, 65–69.
- Gui, Y., Guo, G., Huang, Y., Hu, X., Tang, A., Gao, S., Wu, R., Chen, C., Li, X., Zhou, L., et al. (2011). Frequent mutations of chromatin remodeling genes in transitional cell carcinoma of the bladder. *Nat. Genet.* 43, 875–878.
- Guo, G., Sun, X., Chen, C., Wu, S., Huang, P., Li, Z., Dean, M., Huang, Y., Jia, W., Zhou, Q., et al. (2013). Whole-genome and whole-exome sequencing of bladder cancer identifies frequent alterations in genes involved in sister chromatid cohesion and segregation. *Nat. Genet.* 45, 1459–1463.
- Zarrabi, K., Paroya, A., and Wu, S. (2019). Emerging therapeutic agents for genitourinary cancers. *J. Hematol. Oncol.* 12, 89.
- Miller, M.L., Reznik, E., Gauthier, N.P., Aksoy, B.A., Korkut, A., Gao, J., Ciriello, G., Schultz, N., and Sander, C. (2015). Pan-cancer analysis of mutation hotspots in protein domains. *Cell Syst.* 1, 197–209.
- Gao, J., Aksoy, B.A., Dogrusoz, U., Dresdner, G., Gross, B., Sumer, S.O., Sun, Y., Jacobsen, A., Sinha, R., Larsson, E., et al. (2013). Integrative analysis of complex cancer genomics and clinical profiles using the cBioPortal. *Sci. Signal.* 6, pl1.
- Simonyan, V., and Mazumder, R. (2014). High-performance integrated virtual environment (HIVE) tools and applications for big data analysis. *Genes (Basel)* 5, 957–981.
- Marine, J.C., Bellefroid, E.J., Bourguignon, C., Rivière, M., Lecoq, P.J., Poncelet, D.A., Szpirer, J., Martial, J.A., and Szpirer, C. (1994). Assignment of the human *ZNF83 (HPFI)* zinc finger gene to chromosome 19q13.3-q13.4. *Genomics* 21, 285–286.
- Lupo, A., Cesaro, E., Montano, G., Zurlo, D., Izzo, P., and Costanzo, P. (2013). KRAB-zinc finger proteins: a repressor family displaying multiple biological functions. *Curr. Genomics* 14, 268–278.
- Jen, J., and Wang, Y.-C. (2016). Zinc finger proteins in cancer progression. *J. Biomed. Sci.* 23, 53.
- Hiratsuka, S., Watanabe, A., Sakurai, Y., Akashi-Takamura, S., Ishibashi, S., Miyake, K., Shibuya, M., Akira, S., Aburatani, H., and Maru, Y. (2008). The S100A8-serum amyloid A3-TLR4 paracrine cascade establishes a pre-metastatic phase. *Nat. Cell Biol.* 10, 1349–1355.
- Zhang, X., Ai, F., Li, X., She, X., Li, N., Tang, A., Qin, Z., Ye, Q., Tian, L., Li, G., et al. (2015). Inflammation-induced S100A8 activates Id3 and promotes colorectal tumorigenesis. *Int. J. Cancer* 137, 2803–2814.
- Umezawa, K. (2006). Inhibition of tumor growth by NF- κ B inhibitors. *Cancer Sci.* 97, 990–995.
- Horiguchi, Y., Kuroda, K., Nakashima, J., Murai, M., and Umezawa, K. (2003). Antitumor effect of a novel nuclear factor- κ B activation inhibitor in bladder cancer cells. *Expert Rev. Anticancer Ther.* 3, 793–798.
- Sumitomo, M., Tachibana, M., Ozu, C., Asakura, H., Murai, M., Hayakawa, M., Nakamura, H., Takayanagi, A., and Shimizu, N. (1999). Induction of apoptosis of cytokine-producing bladder cancer cells by adenovirus-mediated I kappa B alpha overexpression. *Hum. Gene Ther.* 10, 37–47.
- Watabe, M., Hishikawa, K., Takayanagi, A., Shimizu, N., and Nakaki, T. (2004). Caffeic acid phenethyl ester induces apoptosis by inhibition of NF κ B and activation of Fas in human breast cancer MCF-7 cells. *J. Biol. Chem.* 279, 6017–6026.
- Kodaira, K., Kikuchi, E., Kosugi, M., Horiguchi, Y., Matsumoto, K., Kanai, K., Suzuki, E., Miyajima, A., Nakagawa, K., Tachibana, M., et al. (2010). Potent cytotoxic effect of a novel nuclear factor- κ B inhibitor dehydroxymethylepoxyquinomicin on human bladder cancer cells producing various cytokines. *Urology* 75, 805–812.
- Kandoth, C., McLellan, M.D., Vandin, F., Ye, K., Niu, B., Lu, C., Xie, M., Zhang, Q., McMichael, J.F., Wyczalkowski, M.A., et al. (2013). Mutational landscape and significance across 12 major cancer types. *Nature* 502, 333–339.
- Faltas, B.M., Prandi, D., Tagawa, S.T., Molina, A.M., Nanus, D.M., Sternberg, C., Rosenberg, J., Mosquera, J.M., Robinson, B., Elemento, O., et al. (2016). Clonal evolution of chemotherapy-resistant urothelial carcinoma. *Nat. Genet.* 48, 1490–1499.
- Dworkin, A.M., Ridd, K., Bautista, D., Allain, D.C., Iwenofu, O.H., Roy, R., Bastian, B.C., and Toland, A.E. (2010). Germline variation controls the architecture of somatic alterations in tumors. *PLoS Genet.* 6, e1001136.
- Gardner, E.E., Lok, B.H., Schneeberger, V.E., Desmeules, P., Miles, L.A., Arnold, P.K., Ni, A., Khodos, I., de Stanchina, E., Nguyen, T., et al. (2017). Chemosensitive relapse in small cell lung cancer proceeds through an EZH2-SLFN11 axis. *Cancer Cell* 31, 286–299.
- Jones, S., Stransky, N., McCord, C.L., Cerami, E., Lagowski, J., Kelly, D., Angiuoli, S.V., Sausen, M., Kann, L., Shukla, M., et al. (2014). Genomic analyses of gynaecologic carcinomas reveal frequent mutations in chromatin remodeling genes. *Nat. Commun.* 5, 5006.
- Munro, D., Ghersi, D., and Singh, M. (2018). Two critical positions in zinc finger domains are heavily mutated in three human cancer types. *PLoS Comput. Biol.* 14, e1006290.
- Stein, J.P., Lieskovsky, G., Cote, R., Groshen, S., Feng, A.C., Boyd, S., Skinner, E., Bochner, B., Thangathurai, D., Mikhail, M., et al. (2001). Radical cystectomy in the treatment of invasive bladder cancer: long-term results in 1,054 patients. *J. Clin. Oncol.* 19, 666–675.
- Mitra, A.P., and Lerner, S.P. (2015). Potential role for targeted therapy in muscle-invasive bladder cancer: lessons from the cancer genome atlas and beyond. *Urol. Clin. North Am.* 42, 201–215, viii.
- Mukherjee, N., Houston, T.J., Cardenas, E., and Ghosh, R. (2015). To be an ally or an adversary in bladder cancer: the NF- κ B story has not unfolded. *Carcinogenesis* 36, 299–306.
- Ran, F.A., Hsu, P.D., Wright, J., Agarwala, V., Scott, D.A., and Zhang, F. (2013). Genome engineering using the CRISPR-Cas9 system. *Nat. Protoc.* 8, 2281–2308.